Calculation of the influence of the absorption grating on the diffraction efficiency in photovoltaic media in reflection geometry for nonlinear regimes

M. A. González-Trujillo[a,b], A. Zúñiga-Segundo[c], I. Casar-Aldrete[d], and J. G. Murillo-Ramírez[a]
[a]*Centro de Investigación en Materiales Avanzados,*
Miguel de Cervantes 120, Complejo Industrial Chihuahua, 31109 Chihuahua, México.
[b]*Departamento de Formación Básica, Escuela Superior de Cómputo, Instituto Politécnico Nacional,*
Unidad Profesional Adolfo López Mateos, México D.F., 07738 México.
[c]*Departamento de Física, Escuela Superior de Física y Matemáticas, Instituto Politécnico Nacional,*
Edificio 9, Unidad Profesional "Adolfo López Mateos", 07738 México, D.F., México.
[d] *Instituto de Física, Universidad Nacional Autónoma de México,*
Apartado Postal 20-364, México, D.F., 01000 México.

Received 3 December 2013; accepted 13 January 2014

With simultaneous phase and absorption gratings, we calculated the contribution of the absorption grating to the total diffraction efficiency in thick samples (around 0.5 cm) of iron doped lithium niobate with an applied electric field between 0 and -400 kV/cm in reflection geometry. We started by solving numerically the set of partial, non-linear, material rate differential equations. Then, we used these solutions to find numerical solutions in a self-consistent way to the beam coupling equations in two-wave mixing along sample thickness. For the given set of values of physical parameters of lithium niobate, we found that the presence of the absorption grating has a weak influence on the diffraction efficiency. It diminishes the total value of the diffraction efficiency in a small amount of around only 1%.

Keywords: Photorefractive gratings; absorption gratings; diffraction efficiency; non linear optics.

Con rejillas simultáneas de fase y de absorción, calculamos la contribución de la rejilla de absorción a la eficiencia total de difracción en muestras gruesas (aproximadamente 0.5 cm) de niobato de litio dopado con hierro. Consideramos la geometría de reflexión, con campos aplicados entre 0 y -400 kV/cm. Primero resolvimos numéricamente el sistema de ecuaciones diferenciales parciales, no lineales del material. Estas soluciones fueron utilizadas luego para calcular el intercambio de energía en la mezcla de dos ondas. Resolvimos numéricamente las ecuaciones del acoplamiento de los haces a lo largo del grosor de la muestra. Para el valor usado del dopaje de hierro, encontramos que la contribución de la rejilla de absorción es menos de 1% del valor total de la eficiencia de difracción.

Descriptores: Rejillas fotorrefractivas; rejillas de absorción; eficiencia de difracción; óptica no lineal.

PACS: 42.65.-k; 42.70-a; 42.70.Nq

1. Introduction

Lithium niobate is an indispensable material that has been used in a large variety of nonlinear optical and photonic devices, and it has been called the "silicon of photonics" [1, 2]. This material is a photovoltaic medium that has a great optical quality and excellent photorefractive properties [3]. On the other hand the volume photorefractive gratings in reflection geometry have been used in a large variety of optical devices, as switchable holographic element [4], in detection of higher nonlinear harmonics for DWDM technology [5] and controllable Fabry-Perot interferometer [6], among many others. Because of its applications, it is very appealing to investigate the light induced charge transport in this material and its photorefractive properties, for example, it has shown how the photorefractive sensitivity can be improved by application of external electric field and different iron doped concentrations [7].

Starting with the fact that the absorption coefficient is proportional to the amount of un-ionized donors [8, 9], in this paper we show that it is possible to calculate the amplitude and phase of the absorption grating. Although the Eq. (3) of Ref. [10] gives the amplitude of the absorption grating (its phase is held fixed), we could not find in the literature an assessment of the influence of an absorption grating on the value of the total diffraction efficiency for reflection geometry. In this work, we are interested on the calculation of the influence of the absorption grating on the value of the total diffraction efficiency for reflection gratings in iron doped lithium niobate.

As it was similarly developed in transmission geometry for a weak applied field (5 kV/cm) [11], we started by solving numerically the set of non-linear material rate differential equations for $LiNbO_3$ to find the full overall space charge field and the ionized donor density, from $t = 0$ seconds up to the stationary state. Afterwards, we used these solutions to calculate the amplitude and phase of the absorption grating. Then, we calculated the diffraction efficiency using a two wave mixing formalism. This latter calculation was performed numerically too. From this strong beam coupling, (with applied electric field between 0 and -400 kV/cm), there is a spatial redistribution of the light intensity pattern. In this way, the grating is spatially non-uniform and its amplitude and phase become a function of crystal thickness. The uniform grating approximation is reasonable for weak coupling or thin-enough crystals. It is not adequate for fiber

like crystals [12], or for strong coupling and high modulation depth [10].

The paper is organized as follows. In Sec. 2 we summarize our theoretical framework in order to identify the parameters which describe the phase and absorption gratings and the photorefractive material equations. In Sec. 3 we show how to calculate the absorption grating for a photorefractive media, which has been solved numerically. In Sec. 4 we numerically calculate the contribution of absorption grating to the diffraction efficiency. Finally a summary and conclusions are given in Sec. 5.

2. Theoretical framework

2.1. Two-wave mixing (TWM) formalism

A general TWM theory in nonlinear media was suggested recently [13]. Their treatment includes both, the volume index (or phase) grating and the gain (or absorption) grating, which have been induced because of the nonlinear response of the medium, when it is illuminated with a static or moving interference pattern. We consider the interaction of two plane, monochromatic, linearly polarized electromagnetic waves, $\vec{A}_1(\vec{r},t)$ and $\vec{A}_2(\vec{r},t)$, that propagate inside a nonlinear media in the paraxial approximation, as shown in Fig. 1. The total light field can then be written as the superposition of them

$$\vec{A}(\vec{r},t) = \vec{A}_1(z)\exp(-i\vec{k}_1\cdot\vec{r} - i\psi_1 t) + \vec{A}_2(z)\exp(-i\vec{k}_2\cdot\vec{r} - i\psi_2 t)\ , \quad (1)$$

where $\vec{k}_1$ and $\vec{k}_2$ are the corresponding wave vectors with wavelengths λ_1 and λ_2 respectively, ψ_1, ψ_2 represents the phases of two light waves, and their amplitudes could be written as $\vec{A}_1(z) = A_{1z}(z)\hat{a}_z + A_{1x}(z)\hat{a}_x$; $\vec{A}_2(z) = A_{2z}(z)\hat{a}_z + A_{2x}(z)\hat{a}_x$, ($\hat{a}_x$ and $\hat{a}_z$ are the unit vectors along x and z direction respectively). The intensity of the moving interference light pattern is

$$I(z) = I_0\left[1 + \mid m \mid \cos(k_g z + \delta t)\right]\ , \quad (2)$$

where $\delta = \psi_2 - \psi_1$, $k_g = \mid \vec{k}_2 - \vec{k}_1 \mid$, $I_0^2 = \mid A_1 \mid^2 + \mid A_2 \mid^2$ is the total intensity of the light and $m(z)$ is the light modulation which varies along the media thickness according to

$$m(z) = 2\frac{A_{1z}(z)A_{2z}^*(z) + A_{1x}^*(z)A_{2x}(z)}{I_0} = \mid m(z) \mid \exp(i\psi_m(z))\ . \quad (3)$$

Note that $\vec{k}_g = \vec{k}_2 - \vec{k}_1$, is the grating vector, which is perpendicular to the fringes recorder in the medium, whose magnitude is $k_g = 2\pi/\Lambda$, where Λ is the grating fringe spacing as is shown in Fig. 1.

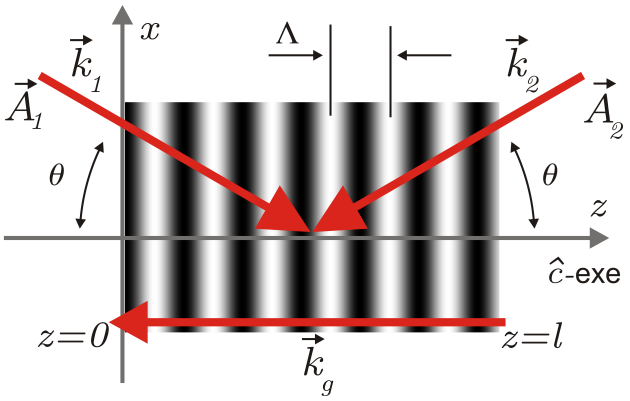

FIGURE 1. Schematic diagram of holographic experiment in the reflection geometry. $\vec{k}_g = \vec{k}_2 - \vec{k}_1$ is the grating vector, which is perpendicular to the fringes recorder in the medium, whose magnitud is $k_g = 2\pi/\Lambda$, where Λ is the grating fringe spacing.

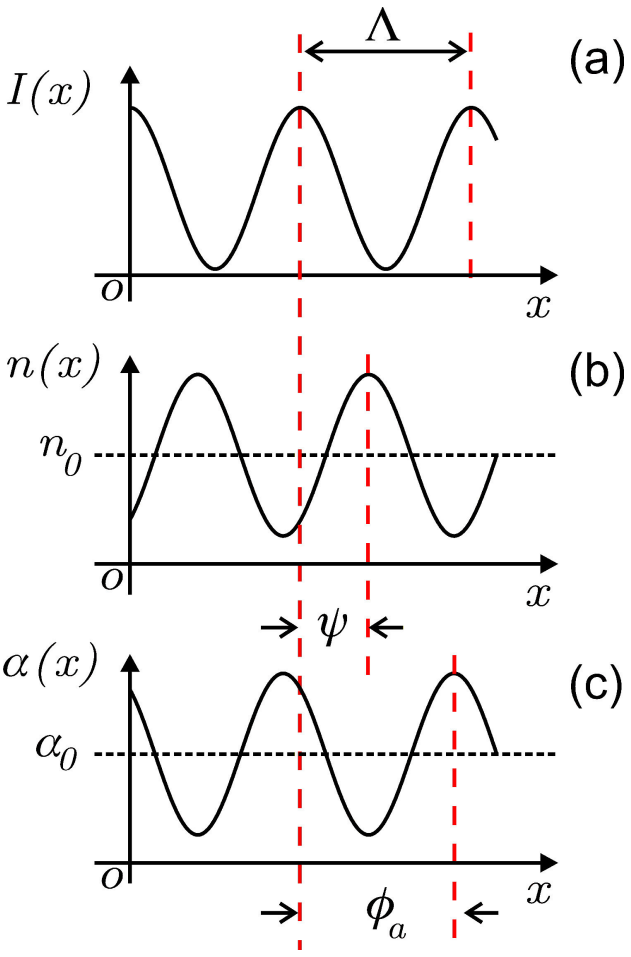

FIGURE 2. (a) Intensity light pattern (b) Refractive index grating (c) Absorption grating. ψ is the phase difference between the phase grating and the interference pattern, and ϕ_a is the phase difference between the absorption grating and the interference pattern.

The aim of beam coupling analysis is to determine the six independent parameters of the index and absorption gratings [14]. In particular, the refractive-index modulation n_1, the absorption modulation α_1 and the phase ϕ between them,

have been already experimentally measured [15]. If a sinusoidal pattern of light (2) is recorded on a photosensitive medium, the refractive index and absorption gratings vary in harmonic way as:

$$n(z) = n_0 + n_1 \cos(k_g z + \delta t + \psi) \,, \tag{4}$$

$$\alpha(z) = \alpha_0 + \mid \alpha_1 \mid \cos(k_g z + \delta t + \phi_a) \,, \tag{5}$$

where n_0 and n_1 are the constant and the modulated refractive indices, and α_0 and α_1 are the constant and the modulated absorption, respectively. In general, the modulations n_1 and α_1 could be functions of time and/or coordinate z. We can see that there is a phase difference ψ between the light pattern and the refractive index grating and another one ϕ_a between the light pattern and the absorption grating, as is shown in Fig. 2.

2.2. Kukhtarev material equations

The photorefractive effect is based on light-induced charge-transport processes. In lithium niobate crystals ($LiNbO_3$), an inhomogeneous illumination excites electrons from defects into the conduction band. These free charge carriers migrate because of diffusion, drift, and the bulk-photovoltaic effect. They are trapped in the darker crystal regions, and space-charge field builds up that modulates the refractive index due to the electro-optic effect [3, 10].

The photorefractive response to illumination of light in photovoltaic media is described by the Kukhtarev material equations [16, 17]:

$$\frac{\partial N_D^+}{\partial t} = (sI + \beta)(N_D - N_D^+) - \tilde{\gamma} n_e N_D^+ \,, \tag{6}$$

$$\frac{\partial n_e}{\partial t} - \frac{\partial N_D^+}{\partial t} = \frac{1}{e} \nabla \cdot \vec{j} \,, \tag{7}$$

$$\vec{j} = e n_e \mu \vec{E} + k_B T \mu \nabla n_e + \tilde{\kappa} s I (N_D - N_D^+) \hat{c} \,, \tag{8}$$

$$\nabla \cdot (\epsilon_o \epsilon E) = e(N_D^+ - N_A - n_e) \,, \tag{9}$$

where s is the photoionization cross section, $\tilde{\gamma}$ the charge carrier recombination rate, e the magnitude of electron charge and μ the mobility of the charge carrier, N_D the donor density, N_D^+ the ionized donor density, N_A the acceptor density, n_e the charge-carrier density, $\vec{j}$ the electric current density, $\tilde{\kappa}$ the glass constant, $\hat{c}$ the +c-axis unit vector along the $z-$direction, $\vec{E}$ the total electric field whose magnitude is given by the sum of the externally applied electric field E_{ext} and the space-charge field E_{sc}, k_B the Boltzmann's constant, T the temperature, t the time, ϵ the dielectric constant, ϵ_o is the permittivity of free space, I the light intensity which is defined in Eq. (2) and finally β the dark generation rate where $I_d = \beta/s$ will be the dark irradiance.

3. Numerical solutions

In this paper, the following parameters of $LiNbO_3$:Fe are used in the calculations [10]: $\mu = 0.8$ cm^{2}V^{-1}s^{-1}, $\tilde{\gamma} = 8.89 \times 10^{-8}$ cm^{3}s^{-1}, $s = 4.6$ cm^{2}s^{-1}W^{-1}, $N_D = 18 \times 10^{18}$ cm^{-3}, $N_A = 1.2 \times 10^{18}$ cm^{-3}, $T = 300$ K, $\tilde{\kappa} = 1.5681 \times 10^{-25}$ A-cm-s, $\epsilon = 30$, $I_d = 0.0$, $I_0 = 0.18$ Wcm^{-2} with $\delta = 0$ and a photovoltaic field $E_{pv} \approx 100$ kVcm^{-1}.

We solved numerically the set of non-linear material rate differential Eqs. (6)-(9), following the method described in Refs. [18, 19], for a fringe spacing of $\Lambda = 0.105$ microns and for several values of the applied field E_{ext} between 0 and -400 kVcm^{-1}. It is necessary to mention that this method does not rely on a Fourier expansion so its validity is not limited to using a truncated harmonic basis. We obtained the overall space charge field $E_{sc}(z,t)$, the ionized donor density $N_D^+(z,t)$ and the charge-carrier density $n_e(z,t)$; for the value of $m_0 = m(z=0) = 1.0, 0.9, 0.6, 0.3$ and 0.1 that is the absolute value of the complex light modulation at the

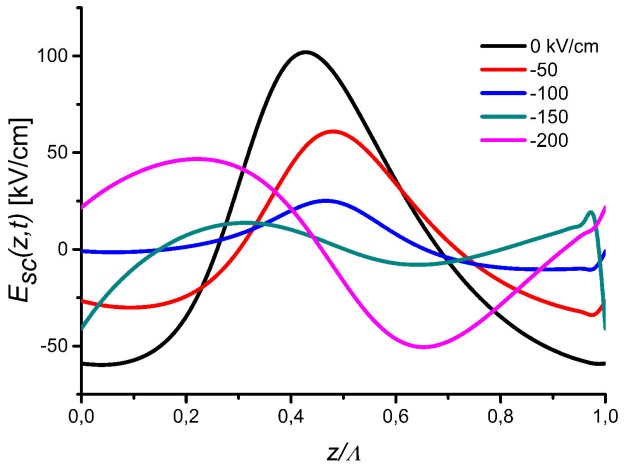

FIGURE 3. Space charge field $E_{\text{sc}}(z,t)$ profile as function of the spatial coordinate z, at $t = 220$ milliseconds, for five applied fields 0, -50,-100,-150 and -200 kV/cm, and a light modulation m = 1.0.

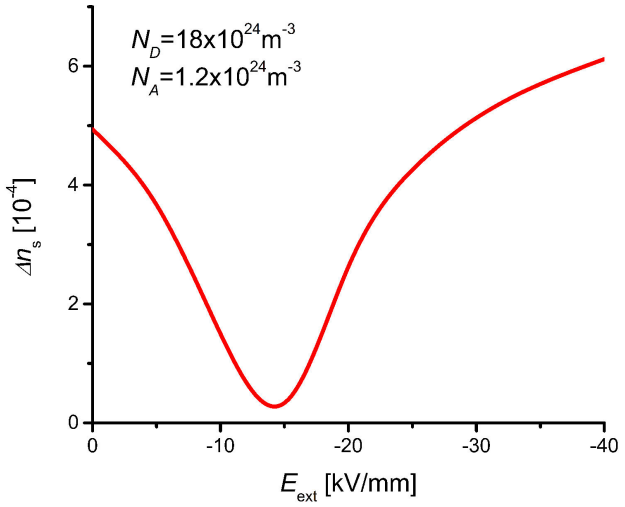

FIGURE 4. Refractive-index change Δn_s for the stationary state as a function of the applied field E_{ext}.

surface of the sample. Then we performed the Fourier decomposition for the calculated overall space charge field to obtain the amplitude E_1, of its fundamental component and its phase, ψ; with respect to the light interference pattern. In this way we have obtained the phase grating strength and its phase as functions of the applied field.

The space charge field $E_{\rm sc}(z,t)$ profile at $t = 220$ milliseconds, obtained for various externally applied electric fields $E_{\rm ext} = 0$, -50,-100,-150 and -200 kV/cm, and light modulation $m_0 = 1.0$ as function of the spatial coordinate z, are presented in Fig. 3. When the applied field is zero the shape of the profile is clearly nonsinusoidal and nonsymmetric. However, when the applied electric field is increased, this shape is gradually lost and the curves are displaced in the counter-direction of applied field. The profile has a tendency to bend around $z = \Lambda$ when the applied field is around -150 kV/cm, which leads to an instability when its absolute value ($\mid E_{\rm ext} \mid$) is slightly higher than photovoltaic field $E_{\rm pv}$. Finally when the applied field is -200 kV/cm the profile is practically sinusoidal but now it is displaced in the direction of applied field. It is interesting to notice that the approximate time to reach the so-called quasi-steady state is about 0.85 seconds, where the first harmonic E_1 reaches saturation. However, at this time we do not have important changes on the final profile of the space-charge field.

The variation of the saturation values of the refractive index changes $\Delta n_s = \frac{1}{2} n_0^3 r_{13} \mid E_1 \mid$ are shown in Fig. 4 as a function of the applied field $E_{\rm ext}$ for fixed donor and acceptor densities N_D and N_A respectively. We see that by increasing the magnitude of applied field the refractive index drops to a minimum and grows afterward when this magnitude is also increases; this behavior is similar to that reported in Ref. [7] with other concentrations of N_D and N_A. We have considered that $2\pi n_o^3 r_{13}/\lambda \approx 1.4\ ^{-1}$, where $n_0 = 2.34$ and $r_{13} = 8.6$ pmV^{-1} are the ordinary refractive index and the electro-optic coefficient respectively for a wavelength $\lambda = 488$ nm [10].

On the other hand, the scaled ionized donor density $N_D^+(z,t)/N_A$ profile after $t = 220$ milliseconds, for light modulation $m_0 = 1.0$ and for various externally applied electric fields ($E_{\rm ext} = 0$, -50,-100,-150 and -200 kV/cm, as in Fig. 3), are present in Fig. 5 as function of the spatial coordinate z. We can see the same kind of behavior that we have seen with the space charge field profile, *i.e.*, the profiles are non-sinusoidal, non-symmetric and when the magnitude of the applied electric field is increased, their shape is displaced in the counter-direction of the applied field. As the absorption in photorefractive medium may be written by the Lambert-Beer relation [8, 9]

$$\alpha = \mathcal{S}(N_D - N_D^+)\ , \tag{10}$$

the constant $\mathcal{S}$ may be determined by calculating the spatial average of Eq. (10), *i.e.*, by means $\langle\alpha\rangle = \alpha_0 = \mathcal{S}(N_D - \langle N_D^+\rangle)$ where α_0 is the average value of the absorption coefficient and $\langle N_D^+\rangle$ is the spatial average of ionized donor density, whose value is different from N_A as it is generally accepted [20] (see Fig. 5). Hence the amplitude of the modulation of the absorption coefficient is:

$$\frac{\mid \alpha_1 \mid}{\alpha_0} = \frac{N_{D-1}^+}{N_D - \langle N_D^+\rangle}\ , \tag{11}$$

where N_{D-1}^+ is the magnitude of the first Fourier coefficient of N_D^+. The values of the amplitude of absorption modulation $\mid \alpha_1 \mid$ are shown in Fig. 6 as a function of the applied electric field $E_{\rm ext}$ for the stationary state. This magnitude will show a behavior very similar to the refractive index changes just discussed. Finally, in Fig. 7 we show the phases of the refractive index and absorption gratings in function of the applied electric field, denoted by ψ and ϕ_a respectively. An interesting characteristic feature is that the phase difference between the

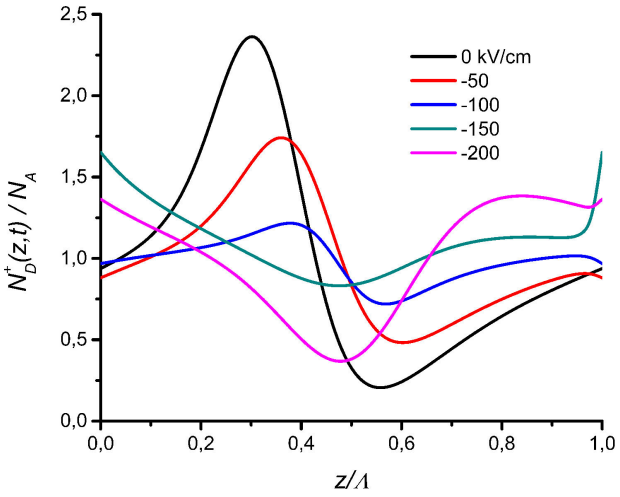

FIGURE 5. Scaled ionized donor density $N_D^+(z,t)$ profile as function of the spatial coordinate z, at $t = 220$ milliseconds, for five applied fields 0,-50,-100,-150 and -200 kV/cm, and a light modulation m = 1.0.

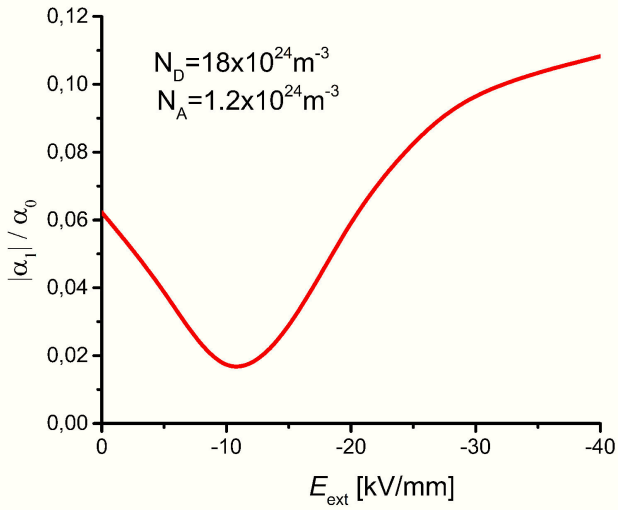

FIGURE 6. Absorption modulation amplitude α_1 for the stationary state as a function of the applied field $E_{\rm ext}$.

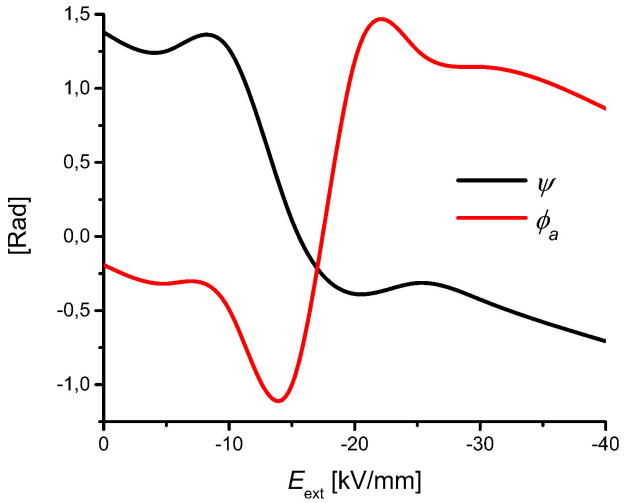

FIGURE 7. Phases of the refractive index grating and absorption grating as a function of the applied field E_{ext}. ψ is the phase difference between the phase grating and the interference pattern, and ϕ_a is the phase difference between the absorption grating and the interference pattern.

index and absorption gratings is slightly different from $\pi/2$ $(-\pi/2)$ when the magnitude of the applied field lies to the left (to the right) of the critical applied field (around -150 kV/cm) at which the refractive-index change is minimum, see Fig. 4.

4. Coupled beam equations

In the reflection geometry, the coupled beam equations are the following [13, 21],

$$\frac{\partial A_1}{\partial z} = -i\left(\kappa^* - i\frac{\alpha_1^*}{2}\right)A_2 - \frac{\alpha_0}{2}A_1 \ , \tag{12}$$

$$\frac{\partial A_2}{\partial z} = i\left(\kappa - i\frac{\alpha_1}{2}\right)A_1 + \frac{\alpha_0}{2}A_2 \ . \tag{13}$$

Where the coupling factors κ and α_1, are calculated from the solution of the material rate equations, since they are due to the space charge field and ionized donor density respectively; notice that we consider them complex and changing along sample thickness z as:

$$\kappa = \frac{\pi}{\lambda\cos\theta}\frac{n_0^3 r_{13} \mid E_1(z) \mid}{2}\exp\left[i(\psi+\psi_m)\right] \ , \tag{14}$$

$$\alpha_1 = \frac{\mid \alpha_1(z) \mid}{\cos\theta}\exp\left[i\phi_a\right] \ , \tag{15}$$

where $\mid \alpha_1 \mid$ is defined in Eq. (11) and θ is the incidence angle in Fig. 1 which is going to be zero. The solutions to the beam coupling Eqs. (12) and (13) must be self-consistent, since the changes in the intensities and phases of the waves cause changes on the light modulation and on the refraction index and these changes in turn, will induce new changes in the intensity and phases of the waves. To obtain these self-consistent solutions we divided the sample in thin layers of thickness Δz [22] in such a way that within each layer the coupling factors are practically constant. This means that we did not allow changes greater that 0.1% within each layer so within each layer, we could have analytical solutions,

$$A_1(z) = \frac{iC_1}{2\kappa - i\alpha_1}(\alpha_0 - \gamma)\exp\left(\frac{1}{2}\gamma z\right) + \frac{iC_2}{2\kappa - i\alpha_1}(\alpha_0 + \gamma)\exp\left(-\frac{1}{2}\gamma z\right) \ , \tag{16}$$

$$A_2(z) = C_1\exp\left(\frac{1}{2}\gamma z\right) + C_2\exp\left(-\frac{1}{2}\gamma z\right) \ , \tag{17}$$

where $\gamma = \sqrt{\alpha_0^2 - \mid \alpha_1 \mid^2 + 4 \mid \kappa \mid^2 - 2i(\kappa^*\alpha_1 + \kappa\alpha_1^*)}$, C_1 and C_2 are constants calculated from the initial values of A_1 and A_2.

When a change of $\mid \kappa(z) \mid$ larger than 0.1% occurred within a layer, we chose a smaller layer and calculated the new corresponding set of values of constants for the corresponding layer Δz. We started evaluating the initial set of constants for the first layer at the surface of the sample by using $\kappa(z=0) = \kappa_0$. Next, for the following layers, the values of the complex amplitudes of the beams at the end of each interval were used to evaluate $m(z)$ and therefore, a new value of κ at z was obtained to use in the following layer. Thus, with the analytical solution within each layer we matched the solutions at the boundaries of the layers.

From the complex amplitudes, obtained from the self-consistent solutions of the pair of beam coupling equations, we calculated the intensities and phases of each wave. We considered no restrictions on the magnitude of the coupling factors given in (16) and (17). From these we calculated the corresponding light modulation $m(z)$ as a function of z, for each sample thickness l. Finally, with the previously recorded $\Delta n_1(z)$, we calculated the diffraction efficiency,

$$\eta(l) = \frac{I_r(0)}{I_i(0)} \ , \tag{18}$$

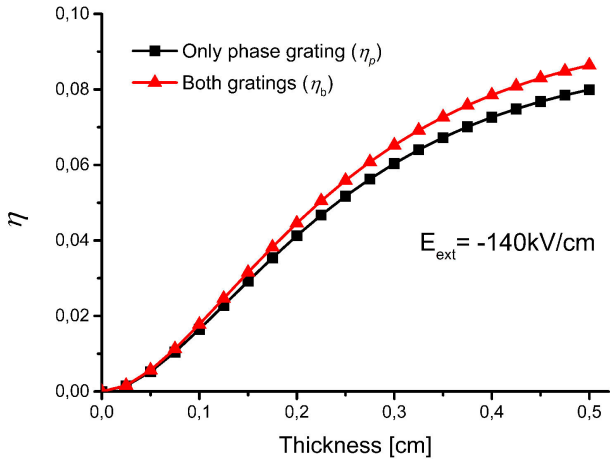

FIGURE 8. Diffraction efficiency as a function of sample thickness. We show the value of η for the phase grating alone and for simultaneous phase and absorption gratings. The largest difference between both values is about 6%.

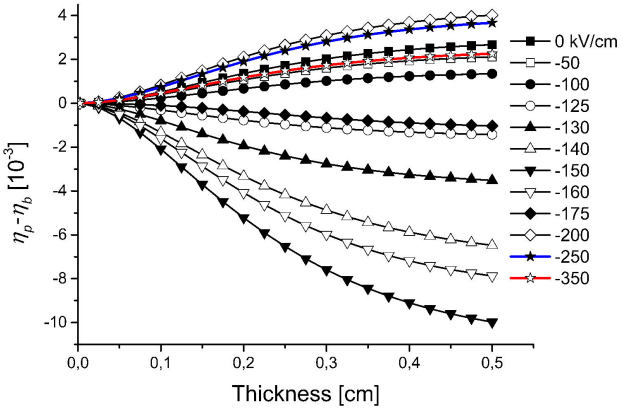

FIGURE 9. Difference $\eta_p - \eta_b$ calculated for different values of thickness and applied external field. η_p and η_b correspond to the diffraction efficiency for phase grating alone and for both (phase and absorption) gratings respectively. Observe that this difference could be positive or negative depending in this case on applied field.

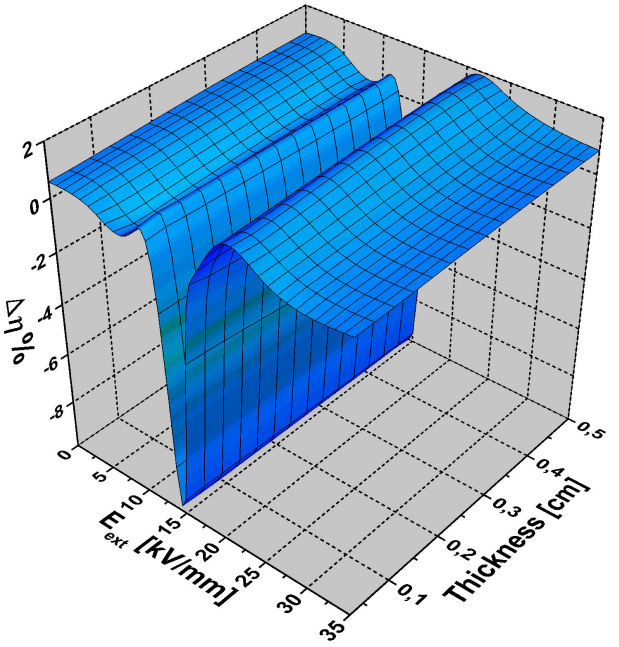

FIGURE 10. $\Delta\eta = (\eta_p - \eta_b)/\eta_p$ calculated for different values of thickness and applied external field. η_p and η_b correspond to the diffraction efficiency for phase grating alone and for both (phase and absorption) gratings respectively.

where $I_i(0)$ is the intensity of the incident light beam for $z = 0$; $I_r(0)$ is the reflected beam intensity at $z = 0$. Notice that we assumed that $I_r(l) = 0$.

In Fig. 8 we show the results for the diffraction efficiency η, as a function of thickness. These results are for a grating with $m_0 = 1$ and applied field $E_{\text{ext}} = -140$ kV/cm. We considered two cases. The first one corresponds to simultaneous phase and absorption gratings (η_b). The second one corresponds to the phase grating alone (η_p). The value of η_b for the first case is a bit larger than the corresponding value for the second case. The largest difference between both values is about $\eta_p - \eta_b = -6\times10^{-3}$ at $l = 0.5$ cm as is shown in Fig. 9. Apparently this difference is reduced for smaller values of thickness, but if we calculate $\Delta\eta = (\eta_p - \eta_b)/\eta_p$ for different values of thickness and applied fields, we can see that this quantity is nearly constant for each value of applied field and it does not depend on the thickness, as it is shown in Fig. 10. $\Delta\eta$ has its minimum ($\approx -10\%$) at $E_{ext} \approx -150$ kV/cm, where the values of photorefractive sensitivity also drops to a minimum [7]. In the high-field region ($E_{ext} \leq -200$ kV/cm) we can see that the presence of the absorption grating has a weak influence on the diffraction efficiency around 1%.

5. Summary and conclusions

For the reflection geometry, we have considered the simultaneous presence of phase and absorption gratings in thick samples (≈ 0.5 cm) of iron doped lithium niobate. In order to assess the importance of the absorption grating on the total value of the diffraction efficiency, we followed several steps. The first was to solve numerically the set of nonlinear differential equation for the material based on the band transport model and included the photovoltaic effect, from 0 seconds up to the stationary state. From the solution, we obtained the full space charge field and the ionized donor density. Then, we performed the Fourier decomposition for each, in this way, we obtained the amplitude E_1, N^+_{D-1}, of their fundamental component and their phases ψ, ϕ_a, with respect to the light interference pattern. These solutions were used to include the non-uniformity of the gratings to calculate the beam energy exchange. Then, we solved numerically the beam coupling equations for recording and for reading in a self-consistent way, to include the variation of light modulation along the sample thickness. From these solutions, we calculated the beam intensities and the the light modulation for recording. Then, we compared the diffraction efficiency when both gratings are present, and when only the phase grating is present. For the set of values given for physical parameters of $LiNbO_3$, we also found that the presence of the absorption grating diminishes or increases the total value of the diffraction efficiency in a very small amount of around 1%.

Our results indicate that the absorption grating cannot strongly affect the index grating in reflection geometry in presence of a static interference pattern in thick samples. In Ref. [10] the formation of refractive-index and absorption gratings was done using a moving interference pattern in thin samples (0.22 mm). In future work we will include in our analysis a non-uniform grating in a thick sample recorded with a moving interference pattern.

Acknowledgments

A.Z.S. would like to thank A. Khomenko and R. Rangel-Rojo (CICESE) for their fruitful discussions, as well as H. Moya-Cessa for his hospitality at INAOE where these ideas were developed. We thank SIP-IPN grant 20140888.

1. M. Kösters, B. Sturman, P. Werheit, D. Haertle, and K. Buse, *Nature Photon. Lett*. **3** (2009) 509.
2. B. Sturman, M. Kösters, D. Haertle, C. Becher, and K. Buse, *Phys. Rev. B.* **80** (2009) 245319.
3. J. Frejlich, *Photorefractive Materials: Fundamental Concepts, Holographic Recording and Materials Characterization*, (Wiley-Interscience, New Jersey 2007).
4. P. Arora, V. M. Petrov, J. Petter, and T. Tschudi, *Optics Comm.* **281** (2008) 1455.
5. P. Arora, V. M. Petrov, J. Petter, and T. Tschudi, *Optics Comm.* **278** (2007) 423.
6. V. M. Petrov, S. Lichtenberg, A.V. Chamrai, J. Petter, and T. Tschudi, *Thin Solid Films* **450** (2004) 178.
7. M. Luennemann, U. Hartwig, and K. Buse, *J. Opt. Soc. Am. B.*, **20** (2003) 1643.
8. K. Buse, *Appl. Phys. B. Lasers and Optics* **64** (1997) 273.
9. L. Solymar and D. J. Cooke, *Volume Holography and Volume Gratings*, (Academic Press, London 1981).
10. M. Luennemann, K. Buse, and B. Sturman, *J. Appl. Phys.* **94** (2003) 6274.
11. L. M. Cervantes, A. Zúñiga, L.F. Magaña, and J.G. Murillo, *Rev. Mex. Fís.* **56** (2010) 323.
12. S. Stepanov, and C. Nuñez-Santiago, *Optics Comm.* **264** (2006) 105.
13. M. Chi, J. -P. Huignard, and P. M. Petersen, *J. Opt. Soc. Am. B.* **26** (2009) 1578.
14. F. Kahmann, *J. Opt. Soc. Am. A.* **10**, (1993) 1562. M. Fally, *J. Opt. Soc. Am. A.* **23** (2006) 2662.
15. M. Fally, M. Ellabban, and I. Drevenšek-Olenik, *Opt. Express.* **16** (2008) 6528.
16. N. V. Kukhtarev, V. B. Markov, S. G. Odulov, M. S. Soskin, and V. L. Vinetskii, *Ferroelectrics* **23** (1979) 949.
17. N. V. Kukhtarev, T. Kukhtareva, and P. P. Banerjee, *Proceedings of the IEEE*. **87** (1999) 1857.
18. J. G. Murillo, L. F. Magaña, M. Carrascosa, and F. Agulló-López, *J. Opt Soc. Am. B.* **15** (1998) 2092.
19. J.G. Murillo, L.F. Magaña, M. Carrascosa, and F. Agulló-López, *J. Appl. Phys.* **78** (1995) 5686.
20. G. Cook, C. J. Finnan, and D. C. Jones, *Appl. Phys. B. Lasers and Optics* **68** (1999) 911.
21. P. Yeh, *Introduction to photorefractive nonlinear optics* (New York: John Wiley & Sons 1993).
22. I. Casar, J. G. Murillo, and L. F. Magaña, *Phys. Lett A.* **352** (2006) 416.